JOURNAL OF PROPULSION AND POWER
Vol. 19, No. 3, May–June 2003

Two-Phase Vorticoacoustic Flow Interactions in Solid-Propellant Rocket Motors

Weidong Cai,* Fuhua Ma,† and Vigor Yang‡
Pennsylvania State University, University Park, PA 16802

Two-phase flow interactions with vorticoacoustic oscillations in simulated solid-propellant rocket motors have been studied numerically using a combined Eulerian–Lagrangian approach. The model accommodates the complete conservation equations in axisymmetric coordinates and, consequently, allows for a detailed treatment of particle dynamics and unsteady motor internal flow evolution. Emphasis is placed on the interphase coupling between the gas and particle fields under the influence of acoustic excitation and turbulence dispersion and the intraphase interactions among particles such as collision and coalescence. The study demonstrates that acoustic oscillations provide additional mechanisms to transfer energy from periodic motions to turbulence, leading to an enhanced level of turbulence intensity and an early transition from laminar to turbulence. On the other hand, turbulence-induced eddy viscosity tends to suppress vortical flow motions caused by acoustic waves. The thermal and momentum relaxation times of particles, along with acoustic characteristic time, play an important role in dictating the two-phase flow interactions with oscillatory motor internal flows. A maximum attenuation of acoustic waves occurs when those timescales become comparable. Small particles, however, usually exert greater influence on the dispersion of acoustic wave through its effective modification of mixture compressibility. Particle intraphase interactions are significant mainly in situations with a wide range of particle size distribution.

Nomenclature

a = speed of sound in pure gas phase
$\bar{a}$ = speed of sound in two-phase gas/particle mixture
C_B = Basset force coefficient
C_d = drag coefficient
C_l = virtual-mass drag coefficient
C_m = mass loading of particles, ρ_p/ρ
C_p = constant-pressure specific heat of gas
C_s = specific heat of particle
C_v = constant-volume specific heat of gas
d_p = particle diameter
e = specific internal energy of gas
e_t = specific total energy of gas
$\boldsymbol{F}_L$ = lift force
$\boldsymbol{F}_p$ = gasdynamic force
f = frequency
h_v = specific enthalpy of particle
J = lift-force coefficient
k_n = wave number
L = chamber length
$\boldsymbol{M}_b$ = Mach number at injection surface
m_i = mass of single particle in group i
m_p = mass of particle
Nu = Nusselt number
n = number density of particles
n_{pi} = number density of particles in group i
Pr = Prandtl number
p = pressure
Q_p = rate of heat exchange between particle and gas
$\boldsymbol{q}$ = heat flux
$\boldsymbol{R}$ = chamber radius or gas constant
Sr = Strouhal number, Rk_n/M_b
T = temperature of gas
T_p = temperature of particle
t = time
$\boldsymbol{U}$ = mean velocity of gas phase
u, v = gas-phase velocity components in axial and radial coordinates, respectively
$\boldsymbol{u}$ = gas velocity
$\boldsymbol{u}_p$ = particle velocity
$\boldsymbol{u}_R$ = relative velocity, $\boldsymbol{u} - \boldsymbol{u}_p$
W_p = work done on particle by gas phase
α = thermal diffusivity of gas
β = total spatial acoustic attenuation coefficient due to two-phase flow interactions, $\beta_\alpha + \beta_v$
β_v = spatial acoustic attenuation coefficient due to two-phase momentum exchange
β_α = spatial acoustic attenuation coefficient due to two-phase heat exchange
γ = ratio of specific heats of gas, C_p/C_v
δ = ratio of gas to particle density, ρ/ρ_s
ε = ratio of imposed acoustic pressure to mean chamber pressure
λ = thermal conductivity of gas
λ_a = acoustic wave length
λ_p = thermal conductivity of particle
μ = dynamic viscosity of gas
ν = kinematic viscosity of gas
ρ = density of gas
ρ_p = bulk density of particles, defined as mass of particles per unit volume of two-phase mixture
ρ_s = density of particle material
$\bar{\rho}$ = effective density of two-phase mixture
τ = viscous stress tensor
τ_a = period of acoustic oscillation
τ_v = momentum relaxation time of particle
τ_α = thermal relaxation time of particle
ϕ = void fraction
$\boldsymbol{\Omega}_p$ = angular momentum of particle
ω = radian frequency

Received 9 September 2002; revision received 17 January 2003; accepted for publication 17 January 2003.

*Ph.D. Student, Department of Mechanical Engineering; currently Siemens Westinghouse Power Corporation, Orlando, FL 32826.
†Ph.D. Student, Department of Mechanical Engineering; mafuhua@psu.edu.
‡Distinguished Professor, Mechanical Engineering; vigor@psu.edu. Fellow AIAA.

Subscripts

a = acoustic component
p = particle phase
v = vortical component

Superscripts

$'$ = fluctuating quantity or correction term due to two-phase flow interaction
$-$ = effective flow property of two-phase mixture

I. Introduction

ALUMINUM particles in solid-rocket propellants serve two purposes: increasing specific impulse and suppressing combustion instability. The damping effect of aluminum particles on motor instability was first recognized in the late 1950s and extensively studied during the 1960s and 1970s.[1,2] Two mechanisms responsible for attenuation of acoustic oscillations have been identified. First, the acoustic energy in a motor can be transferred to and dissipated by particles through the momentum and heat exchange in the two-phase flowfield. Second, the acoustic energy balance in a motor can be substantially modified by the distributed combustion of particles. A general theoretical analysis addressing these phenomena was described by Culick and Yang.[3] The importance of matching particle relaxation time with acoustic characteristic time to maximize the damping efficiency was established. In spite of its broad use in predicting motor stability behavior,[4] the model only considered two-phase flow interactions arising from linear acoustic oscillations. No account was taken of the vortical wave induced by the coupling between the irrotational acoustic and rotational viscous flowfields.[5,6] Furthermore, the influence of turbulence on motor flow evolution was not treated.[7,8] The purpose of the present work is to develop a comprehensive numerical analysis dealing with two-phase flow interactions in rocket motors with acoustic oscillations. Emphasis is placed on the momentum and energy transfer between the gas and particle phases under conditions with and without the presence of turbulence. The study is limited to cold-flow simulations, such that various fundamental fluid-dynamic processes dictating the two-phase vorticoacoustic flow evolution can be identified unambiguously.

In view of the limitations of analytical treatment of two-phase motor flows, especially for problems involving complex grain configurations and turbulent transport, much effort was recently devoted to numerical studies. A variety of problems, such as slag accumulation,[9,10] distributed combustion of aluminum particles,[11,12] two-phase interactions under oscillatory conditions,[13,14] and stability of acoustic waves in two-phase flows[15] were carefully examined. Substantial knowledge was obtained about particle dynamics and combustion as well as their interactions with motor flows. An informative review of the state of art was given by Dupays et al.[16] The existing work, however, does not include the oscillatory flowfield near the chamber wall, where vorticity generation and transport plays a dominant role in dictating the motor flow evolution. The present paper attempts to remedy this deficiency by conducting a unified two-phase flow analysis capable of addressing these fundamental issues. The interactions among particle dynamics, flow oscillations, and turbulent motions throughout the entire motor and their collective effect on motor stability behavior will be examined systematically.

The oscillatory flowfield in a rocket motor consists of three distinct types of wave motions: acoustic (irrotational and compressible), vortical (rotational and incompressible), and entropy (arising from unsteady heat release) modes.[5–8,17,18] The coupling between the acoustic wave and the incoming radial mass flow from the propellant surface generates fluctuating vorticity and, consequently, causes energy transfer from the acoustic to the vortical field, a phenomenon commonly known as the flow-turning energy loss.[3] The interactions between entropy fluctuations and nonuniform motor flows may act as a strong source term for driving acoustic oscillations in regions with large velocity gradients.[18] The three waves, along with the transient combustion response of propellant, collectively dictate the stability behavior of a rocket motor. Turbulence plays an important role in determining the wave characteristics through the damping effect of turbulence-induced eddy viscosity on vortical motion.[6,8] In addition, the interactions between organized oscillatory motions and turbulent fluctuations give rise to additional mechanisms of energy production, transfer, and dissipation in each of the three wave modes.[8] The situation is further complicated by the presence of aluminum particles due to two-phase interactions and distributed combustion. Particles may deviate from their mean flow paths under the influence of gas flow oscillations and turbulence dispersion and, consequently, enhance the intraphase interactions in the particle field by means of particle collision and agglomeration. The preceding phenomena were only studied partially or separately in the past. Little effort has been made so far to address their integrated effect, especially under conditions representative of operational rocket motor environments.

This paper focuses on the two-phase flow interactions in a solid rocket motor with acoustic excitations. Chemical reactions are not included to allow for a detailed investigation of motor flow dynamics without complications arising from the surface and distributed combustion of propellant and metal particles. The analysis is based on a combined Lagrangian and Eulerian approach for the particle and gas phases, respectively. An improved two-equation model that takes into account the effects of wall transpiration, flow unsteadiness, and two-phase interactions is developed to achieve turbulence closure. The main objectives of the present work are 1) to study particle dynamics in the presence of turbulent and acoustic oscillations in the gas phase, 2) to examine the interactions between turbulent and organized oscillatory flows, 3) to explore the attenuation and dispersion effects of particles on unsteady flow motions, and 4) to investigate intraphase interactions among particles including collision and coalescence.

II. Theoretical Formulation

The physical model consists of an axisymmetric chamber with a closed head end, as shown in Fig. 1. Premixed nitrogen gas and aluminum particles are uniformly injected along the azimuth to simulate the evolution of combustion products of a metallized composite propellant. Standing acoustic waves are introduced to the chamber by imposing periodic pressure oscillations at the exit of the chamber.

Governing Equations for Gas Phase

The formulation for the gas phase is based on the conservation equations of mass, momentum, and energy in axisymmetric coordinates. When chemical reactions are neglected, these equations can be written in the following conservative form.

Mass:

$$\frac{\partial(\phi\rho)}{\partial t} + \nabla\cdot(\phi\rho\boldsymbol{u}) = 0 \tag{1}$$

Momentum:

$$\frac{\partial(\phi\rho\boldsymbol{u})}{\partial t} + \nabla\cdot(\phi\rho\boldsymbol{u}\boldsymbol{u}) = -\nabla(\phi p) + \nabla\cdot(\phi\tau) - \sum_i \boldsymbol{F}_{pi} n_{pi} \tag{2}$$

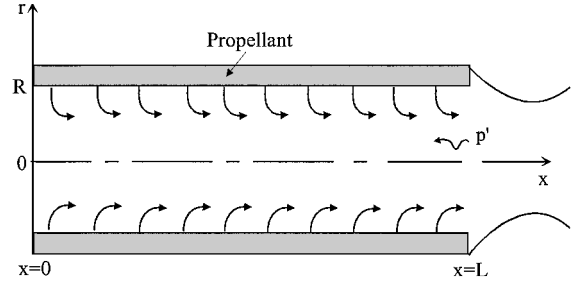

Fig. 1 Schematic diagram of a solid rocket motor.

Energy:

$$\frac{\partial(\phi\rho e_t)}{\partial t} + \nabla\cdot[\phi(\rho e_t + p)\boldsymbol{u}]$$
$$= -\nabla\cdot(\phi\boldsymbol{q}) + \nabla\cdot(\phi\tau\cdot\boldsymbol{u}) - \sum_i W_{pi}n_{pi} - \sum_i Q_{pi}n_{pi} \quad (3)$$

where τ is the stress tensor. The specific total energy e_t and heat transfer rate $\boldsymbol{q}$ are defined respectively as follows:

$$e_t = e + \boldsymbol{u}\cdot\boldsymbol{u}/2, \qquad \boldsymbol{q} = -\lambda\nabla T \quad (4)$$

The void fraction ϕ is assumed to be unity because the volume occupied by particles is exceedingly small compared with that of the gas phase. The source term

$$-\sum_i Q_{pi}n_{pi}$$

in the energy equation denotes the rate of heat transfer from the particle to the gas phase, and

$$-\sum_i W_{pi}n_{pi}$$

stands for the work done on the gas phase by particles, with n_{pi} representing the number density of particles in group i. Specific expressions of $\boldsymbol{F}_{pi}$, W_{pi}, and Q_{pi} will be given in a later section.

Turbulence Closure

An improved two-layer model taking into account the wall transpiration effect is employed to achieve turbulence closure. The approach employs the standard k–ε model for regions away from the wall and a one-equation model for the near-surface region. Because surface mass injection tends to reduce the wall damping effect, turbulence length scales close to the wall are modified following the approach described in Ref. 19.

The two-equation turbulence models are conventionally calibrated for flows under steady-state conditions. Direct application of these models to unsteady flow motions remains questionable. To clarify this issue, a series of experiments have been performed to study turbulence intensities in boundary layers with external oscillations. Cousteix et al.[20] concluded that, although the measured turbulence intensities and Reynolds shear stresses may change significantly during oscillations, the ratio of the shear stress to its component turbulence intensity remains fixed at a value equivalent to that in a steady flow. Thus, under certain circumstances, especially for relatively low-frequency oscillations, a steady-flow turbulence model may be used to predict unsteady turbulence behavior. When the oscillation frequency exceeds a critical value, significant interactions between oscillatory motions and turbulence structures may occur, as observed experimentally by Ramaprian and Tu.[21] These interactions may seriously compromise the validity of turbulence models. Several studies have been performed to address this issue. For wall-bounded flows with impressed velocity oscillations, the flow near the wall responds quite readily to external forcing and manifests itself with a rapid phase change of flow quantities. On the other hand, the outer region of the boundary layer is not as responsive as the inner layer and behaves in a quasi-steady manner. This observation suggests that only the near-wall treatments in turbulence models need to be modified to account for flow unsteadiness.

Fan and Lakshminarayana[22] developed a low Reynolds number turbulence model accommodating flow oscillations, in which the local turbulence characteristic velocity (or the local Reynolds number), instead of the inner variable y^+, was used in the formulation of near-wall functions. The model correctly predicts the unsteady near-wall velocity profile and the unsteady skin function in turbulent boundary layers at various oscillation frequencies. Following the same approach, the present work extends the two-layer turbulence model described in Ref. 19 to account for flow unsteadiness by modifying the inner-layer turbulence length scale. The work is based on the experimental study by Kovalnogov,[23] in which the heat transfer and friction in unsteady turbulent flows with longitudinal pressure gradients were investigated. A detailed description of the treatment is given by Cai.[24] The modulation of the turbulence structure by the particle phase is formulated using the model developed by Mostafa and Mongia.[25]

Governing Equations for Particle Phase

Particle dynamics is modeled using a Lagrangian approach. To facilitate numerical calculations, individual particles are treated collectively as a "parcel," which represents a family of physical particles having identical size, velocity, and temperature at the same location. The quantity of particles in each parcel is determined by the particle loading density. Each particle is governed by Newton's second law and energy conservation law:

$$\frac{\mathrm{d}\boldsymbol{x}_p}{\mathrm{d}t} = \boldsymbol{u}_p, \qquad m_p\frac{\mathrm{d}\boldsymbol{u}_p}{\mathrm{d}t} = \boldsymbol{F}_p, \qquad m_pC_s\frac{\mathrm{d}T_p}{\mathrm{d}t} = Q_p \quad (5)$$

where $\boldsymbol{x}_p$, $\boldsymbol{u}_p$, m_p, and T_p are the particle displacement, velocity, mass, and temperature, respectively. Following the approach of Faeth,[26] an order-of-magnitude analysis of the various forces on particles is conducted. The numerical result given in Table 1 is based on the flow conditions representative of an operational solid rocket motor as described in Ref. 3. The density ratio ρ_s/ρ ranges from 200 to 500 and particle size from 2 to 400 μm in diameter.

If we ignore the virtual-mass and Basset forces due to their small magnitudes and the Magnus force due to the lack of knowledge about particle angular momentum, the resultant force acting on a particle is simplified as

$$\boldsymbol{F}_p = (\pi/8)C_d\rho d_p^2|\boldsymbol{u}_R|\boldsymbol{u}_R + \boldsymbol{F}_L \quad (6)$$

The drag coefficient C_d is determined based on Putnam's work.[28] The work done by a particle on the surrounding gas is expressed as

Table 1 Forces on particles in solid rocket motors[a]

Forces	Formula	Ratio to drag force	Ratio to drag force
Drag force[26]	$\frac{\pi}{8}C_d d_p^2\rho\lvert\boldsymbol{u}_R\rvert\boldsymbol{u}_R$	1	1
Virtual-mass force[26]	$\frac{\pi}{12}C_I d_p^3\rho\frac{\mathrm{d}\boldsymbol{u}_R}{\mathrm{d}t}$	$\left(\frac{\rho}{\rho_s}\right)$	$10^{-3}\sim10^{-2}$
Basset force[26]	$\frac{3}{2}d_p^2(\pi\rho\mu)^{\frac{1}{2}}C_B\times\int_{t_o}^{t}\frac{1}{(t-\xi)^{\frac{1}{2}}}\frac{\mathrm{d}\boldsymbol{u}_R}{\mathrm{d}\xi}\mathrm{d}\xi$	$\left(\frac{\rho}{\rho_s}\right)^{\frac{1}{2}}$	$10^{-2}\sim10^{-1}$
Magnus force[26]	$\frac{\pi}{8}\rho d_p^3\boldsymbol{\Omega}_p\times\boldsymbol{u}_R$	$\frac{\lvert\boldsymbol{\Omega}_p\rvert d_p^2}{24\nu}$	Less than lift force
Lift force[27]	$1.6\rho\nu^{\frac{1}{2}}d_p^2\lvert\boldsymbol{u}_R\rvert\left\lvert\frac{\partial u}{\partial y}\right\rvert^{\frac{1}{2}}\times\mathrm{sign}\left(\frac{\partial u}{\partial y}\right)\boldsymbol{J}$	$\left[\frac{d_p^2(\partial u/\partial y)}{\nu}\right]^{\frac{1}{2}}J$	$0\sim10$

[a]Density ratio $200\le\rho_s/\rho\le500$ and diameter $2\le d_p\le400$ μm.

$$W_p = \boldsymbol{F}_p \cdot \boldsymbol{u}_p \tag{7}$$

The convective heat transfer between the particle and gas phases is

$$Q_p = \pi d_p N u \lambda (T - T_p) \tag{8}$$

where the Nusselt number is calculated using Whitaker's formula.[29]

The effect of turbulence on particle dynamics is treated using the stochastic separated flow (SSF) model developed by Shuen et al.,[30] in which particles are assumed to interact with a succession of turbulent eddies as they move through the computational domain. The duration of interaction between an eddy and a particle is determined from the smaller one between the eddy life time and the transit time required for a particle to traverse the eddy. The assumption of isotropic turbulence in the SSF model is justified by the studies of Chen and Pereira[31] and Burry and Bergeles,[32] in which two improved SSF models were developed to account for turbulence anisotropy. Results indicate that the use of anisotropic scales exerts minor influence in predicting the mean velocity and turbulent kinetic energy of the particle phase.

Particle Collision, Breakup, and Coalescence

Metal particles usually appear as liquid droplets in the high-temperature environment of a rocket motor. To simulate particle collisions caused by acoustic oscillations and turbulent dispersion, the model proposed by Salita[33] is introduced, in which two scenarios are suggested after the collision of two particles: stable coalescence and temporal coalescence followed by separation, with the final separated particles being identical to the incident droplets. The condition for stable coalescence is that the rotational energy due to collision is less than the surface energy required to hold the agglomerated particle, and a critical resultant angular momentum is proposed according to Salita's work. The condition for particle breakup is based on the broken balance between drag force and surface tension and can be characterized using a critical Weber number We_c as summarized by Lefebvre.[34] Two identical smaller particles are produced with the same flow properties after breakup.

III. Numerical Scheme

A characteristic trait of rocket motor internal flows is that the gas velocity in the bulk of the computational domain is much smaller than the acoustic speed. Therefore, conventional numerical algorithms developed for compressible flows may encounter two major difficulties: 1) disparity of the eigenvalues of the system and 2) singular behavior of the pressure gradient in the momentum balance. To circumvent these difficulties, a preconditioning technique in conjunction with an implicit dual time-stepping integration method as detailed in Ref. 35 is employed in the present study. The scheme has proven to be quite efficient and robust over a wide range of Mach numbers and can achieve a high degree of temporal accuracy with only a modest increase in computation cost. Moreover, because the governing equations are solved implicitly, the numerical method is very stable and allows the selection of the integration time step to be dictated by physical processes rather than numerical stability.

The Runge–Kutta–Gills method was chosen for solving the particle-phase governing equations. The physical time step for the particle-phase calculation is less than $\frac{1}{10}$ of the momentum relaxation time. Computation of the two-phase flow is conducted in a fully coupled manner, with the source terms associated with two-phase interactions updated at every gas-phase computational iteration.

IV. Attenuation and Dispersion of Acoustic Waves by Particles

Epstein and Carhart[36] established an analytical model, which was later validated by the experiments of Zink and Delsasso,[37] to quantify the attenuation and dispersion of acoustic waves by rigid particles in a gaseous medium. The analysis was recently generalized by Temkin[38,39] to accommodate the particle compressibility produced by the relative motions between host fluid and particles. Thus, the resultant theory is applicable to aerosols, bubbly liquids, emulsions, and hydrosols.

By following the approach of Epstein and Carhart,[36] the spatial attenuation coefficient due to two-phase momentum exchange β_v is given by

$$\beta_v = (3\pi n d_p/a)\nu(1+Y)I_v \tag{9}$$

where

$$I_v = 16Y^4/[16Y^4 + 72\delta Y^3 + 81\delta^2(1+2Y+2Y^2)] \tag{10}$$

with

$$Y^2 = \omega d_p^2 \big/ 8\nu = \tfrac{9}{4}(\rho/\rho_s)\omega\tau_v, \qquad \delta = \rho/\rho_s \tag{11}$$

The momentum relaxation time of particle τ_v is defined as

$$\tau_v = \rho_s d_p^2 \big/ (18\rho\nu) \tag{12}$$

It characterizes the time required for a particle to reach momentum equilibrium with the ambient fluid in response to a local flow variation.

The spatial attenuation coefficient due to the irreversible flow of thermal energy between the gas and particle phases β_α is given by

$$\beta_\alpha = (2\pi n d_p/a)\alpha(\gamma-1)(1+Z)I_\alpha \tag{13}$$

where

$$I_\alpha = 4Z^4 \big/ \left[4Z^4 + 12\delta(C_p/C_s)Z^3 + 9\delta^2(C_p/C_s)^2\right] \tag{14}$$

with

$$Z^2 = \omega d_p^2 \big/ 8\alpha = \tfrac{3}{2}(\rho/\rho_s)(C_p/C_s)\omega\tau_\alpha = \tfrac{9}{4}(\rho/\rho_s)Pr\,\omega\tau_v$$
$$\alpha = \lambda/\rho C_p \tag{15}$$

The thermal relaxation time of particle τ_α is defined as

$$\tau_\alpha = \rho_s C_s d_p^2 \big/ (12\rho C_p \alpha) \tag{16}$$

which characterizes the time required for a particle to reach thermal equilibrium with the ambient fluid in response to a local flow variation. Clearly, both I_v and I_α depend on the frequency of acoustic oscillation, density ratio, and particle relaxation times. With appropriate manipulations of Eqs. (9) and (13), the total acoustic attenuation coefficient due to two-phase interactions, $\beta(=\beta_v+\beta_\alpha)$, can be obtained as

$$\beta\lambda_a = (2\pi/\omega\tau_v)C_m\left[(1+Y)I_v + (1+Z)(\gamma-1)I_\alpha \big/ \left(\tfrac{3}{2}Pr\right)\right] \tag{17}$$

where λ_a is the wave length of acoustic oscillation and C_m the particle mass fraction, defined as the mass ratio of particle to gas phase per unit volume of the two-phase mixture.

The acoustic wave speed is determined by assuming that the two-phase mixture can be treated as a perfect gas with its thermodynamic properties modified by the presence of particles,

$$\bar{a}^2 = \bar{\gamma}\bar{R}\bar{T} = \frac{\bar{C}_p}{\bar{C}_v}\frac{p}{\bar{\rho}} = \frac{(C_v + C_v' + R)}{(C_v + C_v')}\frac{p}{(\rho+\rho')} \tag{18}$$

where the overbar denotes the effective property of the two-phase mixture and the prime the correction term resulting from two-phase interactions. For a dilute particle-laden flow with a low or moderate particle mass fraction, to first-order approximation, modifications of the density and specific heat can be written as

$$\rho' = \rho C_m(1-I_v), \qquad C_v' = C_s C_m(1-I_\alpha) \tag{19}$$

Substitution of Eq. (19) into Eq. (18) and neglect of higher-order terms gives rise to the following equation for quantifying the change of acoustic velocity caused by the presence of particles:

$$\Delta a = a - \bar{a} \approx (aC_m/2)\left(C_s R \big/ C_p^2\right)(1-I_\alpha) + (aC_m/2)(1-I_v) \tag{20}$$

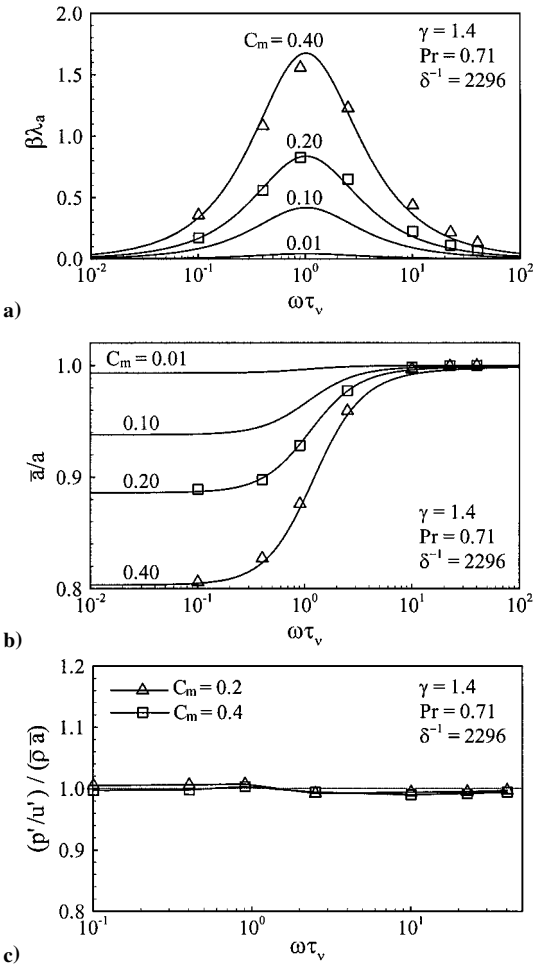

Fig. 2 Effect of particles on a) attenuation, b) dispersion, and c) impedance of acoustic waves in two-phase mixtures: △ and □, numerical simulation, and ——, theoretical prediction.

The first term on the right-hand side accounts for the velocity change due to the increase in heat capability, an effect directly related to the enhanced compressibility of the mixture. The second term is responsible for the particle dispersion effect associated with viscous damping.

As part of the model validation effort, the attenuation and dispersion of acoustic waves by particles in a channel flow is studied. The physical model measures 1.88 m in length and 0.1 m in height. The mean pressure and temperate are 1 atm and 300 K, respectively. Periodic pressure oscillations with a magnitude of 1% of the mean value is imposed at the entrance where premixed air and aluminum particles flow in. Nonreflecting boundary conditions are applied to the exit to allow for traveling acoustic waves in the channel. Figure 2a shows good agreement of the spatial attenuation coefficient of the acoustic wave between the numerical predictions and the theory of Epstein and Carhart[36] over a wide range of oscillation frequency, particle size, and loading density. The open symbols and solid lines denote numerical and theoretical values, respectively. There exists an optimum particle size with $\omega\tau_v = 1$ at which the maximum damping of acoustic motion occurs. For tiny particles that can closely follow wave motions with $I_v = I_\alpha \approx 0$, the relative velocity and temperature differences between the two phases become so small that the viscous and thermal dissipation is insignificant. On the other hand, large particles with $I_v = I_\alpha \approx 1$ can hardly follow the wave motions to cause effective momentum and energy exchange, thereby leading to negligible acoustic attenuation. Only particles between these two extremes exert dissipation on wave motions.

This observation can also be conceived in the particle dispersion effect, as shown in Fig. 2b. Propagation of acoustic waves in a particle-filled gas medium involves a series of rarefaction and compression processes, during which both momentum and thermal exchanges take place between particles and neighboring gases. For small particles, equilibria with surrounding gases can be easily reached to allow particles to be treated as an additional gaseous species. For particles with relaxation times much greater than the period of acoustic wave, however, the large thermal inertia prohibits effective energy transfer between the gas and particles. The compressibility of the gaseous medium remains almost unchanged, and the acoustic wave speed has a value corresponding to that in a pure gas. Note that this result bears a strong resemblance to that given in Ref. 3 (p. 754) using a different approach, in which the particle relaxation effects are incorporated in a unified theory for treating combustion instabilities in two-phase mixtures. Excellent agreement of the acoustic wave speed is obtained for small $\omega\tau_v$ and C_m. The theory in Ref. 3, however, underpredicts the speed of sound by 4% for $C_m = 0.4$ in the limit of $\omega\tau_v \to \infty$.

Figure 2c shows the acoustic impedance of the two-phase mixture, $\overline{\rho a}$, as a function of the nondimensional frequency and particle mass fraction. The effective mixture density and speed of sound are determined according to Eqs. (19) and (20). For low frequencies or small particles, $\omega\tau_v \to 0$, the effective density $\bar{\rho}$ approaches its asymptotic value of an equilibrium flow, with $\bar{\rho} = \rho(1 + C_m)$. On the other hand, if the frequency is relatively high or the particles are large, that is, $\omega\tau_v \to \infty$, the density correction term ρ' vanishes and $\bar{\rho}$ simply takes the value of the pure phase, with $\bar{\rho} = \rho$.

V. Gas-Phase Motor Internal Flow Development

As a specific example, the Culick/Yang research motor[3] is employed in the present study. The chamber measures 5.1 cm in diameter and 0.6 m in length. The mean chamber pressure is 100 atm, and the mean temperature of 3500 K corresponds to the adiabatic flame temperature of a metallized ammonium perchlorate/hydroxyl terminated polybutadine (AP/HTPB) solid propellant. Air and aluminum particles are injected through the walls to simulate the flow evolution of the combustion products. The air mass flux of 20.2 kg/m · s is obtained based on the measured propellant burning rate of 11.2 mm/s and density of 1800 kg/m^3. The corresponding injection Mach number based on the surface injection velocity is 1.7×10^{-3}. The turbulent kinetic energy k_w and its dissipation rate ε_w at the surface are specified following the approach of Beddini,[40] which accounts for the effects of surface roughness and initial turbulence intensity,

$$k_w = \sigma_v^2 |v_w|^2, \qquad \varepsilon_w = C_u^{\frac{3}{4}} k_w / l_w \tag{21}$$

where v_w is the surface injection velocity and σ_v a parameter characterizing the surface roughness, which is assigned a value of 0.035. C_u is an empirical constant set to 0.09. The characteristic length scale of turbulence, l_w, is taken to be 200 μm in the present study.

Periodic pressure oscillations with amplitudes of 2% of the mean value are imposed at the exit to generate longitudinal standing acoustic waves in the chamber. The computational grid for the gas phase consists of 70 and 140 points in the axial and radial directions, respectively. The grids are clustered near the injection surface to resolve the vortical wave structure and turbulent boundary layer. The smallest grid near the wall corresponds to $y^+ = 5$, and each vortical wavelength is covered by at least 10 grids. Attention is also given to the resolution of the vortical wave in the core-flow region where the wave length diminishes due to the vanishing mean-flow radial velocity near the centerline of the chamber.[5]

Stationary Flowfield

Figure 3 shows the distributions of the Mach number and turbulence properties under a steady-state condition. The overall flow development in the chamber can be characterized by three distinct regimes: laminar, transitional, and fully developed turbulent flow, as elucidated in Refs. 7, 40, and 41. The flow is predominantly laminar in the upstream regime and undergoes transitions to turbulence at $x = 0.2$ m as a result of hydrodynamic instability. Unlike channel flows without surface mass injection, the outbreak of turbulence occurs away from the walls. The peak in turbulence intensity moves closer to the wall in the downstream direction until the surface injection prohibits further penetration of turbulence. As the flow develops

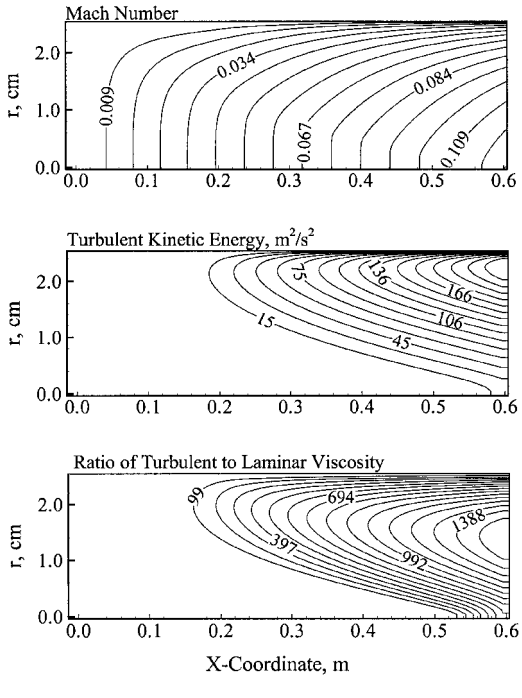

Fig. 3 Steady-state condition contour plots of a) Mach number, b) turbulent kinetic energy, and c) ratio of turbulent to laminar viscosity.

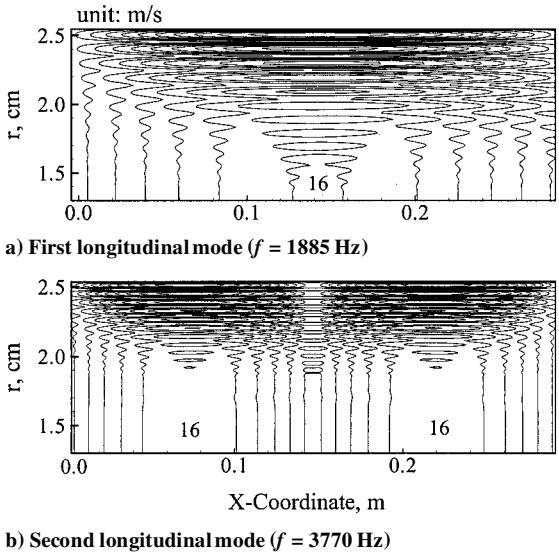

Fig. 4 Contour plots of amplitude of axial velocity fluctuation in laminar flow.

farther downstream, the velocity profile transits into the shape of a fully developed turbulent pipe flow with surface mass injection. The axial velocity becomes much steeper near the wall, but smoother in the core region.

Acoustic and Shear Flowfields

In the present nonreacting flow study, the oscillatory flowfield in the chamber involves only acoustic and vortical motions. To provide direct insight into the wave interactions without complications arising from turbulence, we first treat a short chamber with a length of 0.3 m, in which the flow is predominantly laminar. Figure 4 shows the contour plots of the amplitude of the axial-velocity fluctuation for the first two longitudinal modes. The corresponding frequencies are 1885 and 3770 Hz, respectively. Only the upper portion near the wall is presented to achieve better spatial resolution. The complex structure adjacent to the surface indicates the existence of an acoustic boundary layer, within which rapid velocity fluctuations associated with unsteady shear (or vorticity) waves occur.[5–8]

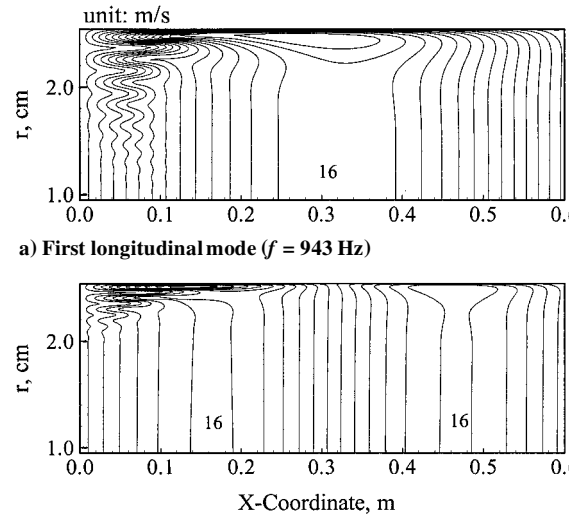

Fig. 5 Contour plots of amplitude of axial velocity fluctuation in both laminar and turbulent flows.

Vorticity disturbance is produced at the lateral boundary to satisfy the no-slip condition for a viscous flow. It then propagates inward at the local flow velocity and is finally damped out by viscous dissipation. Consequently, a simple acoustic field is rendered in the core-flow region, with a one-dimensional distribution of the velocity fluctuation, which can be accurately predicted using classical acoustic theory. Because the viscous damping effect on the vorticity wave is proportional to the oscillation frequency,[5,6] the acoustic boundary-layer thickness, defined by the vertical location at which the shear wave amplitude decays to less than 1% of the acoustic velocity amplitude, of the first mode is about two times greater than that of the second mode, as evidenced in Fig. 4.

The full-scale Culick/Yang[3] research motor measuring a length of 0.6 m is employed to study the interactions between a stationary turbulent flow and acoustic oscillation. Figure 5 shows the distributions of the amplitude of the axial velocity fluctuation of the first two longitudinal modes at the frequencies of 943 and 1885 Hz, respectively. Compared with its counterpart in the upstream laminar region, the vorticity wave in the downstream turbulent region is considerably damped out by the turbulence-inducededdy viscosity. Turbulence can effectively smear out any organized disturbance generated from the surface within a short distance, rendering a nearly one-dimensional oscillatory field in the bulk of the chamber except for a thin acoustic boundary layer near the surface. A thorough discussion of this subject may be found in Refs. 6 and 8.

On the other hand, acoustic oscillations exert strong influence on unsteady flow evolution. In particular, a single-harmonic oscillation may excite a fluctuating flow with a broadband frequency spectrum, a phenomenon referred to as acoustically induced turbulent motions. Generation of turbulence by organized external forcing can be viewed as an energy transfer process from the acoustic to the turbulent flowfield. Apte and Yang[8] showed in their large-eddy simulations of injection-driven flows that the coupling between the Reynolds stress and the spatial gradient of the acoustic velocity provides a mechanism to transfer the kinetic energy from acoustic motions to turbulent fluctuations. Furthermore, an early transition from laminar to turbulence may occur, depending on the forcing amplitude and frequency. In general, the effect of energy exchange tends to be more profound for low-frequency acoustic oscillations and can be characterized using a nondimensional parameter, $k\sqrt{(f\nu)}/a$, where k is a constant scaling factor. Figure 6 shows the radial distributions of time-averaged turbulence kinetic energy at various axial locations for the first longitudinal mode. The corresponding property of a stationary flow is also included for comparison. An enhanced level of turbulence due to acoustic excitation is clearly observed. The acoustic wave can indeed induce flow instability and cause transfer of energy from the organized to the turbulent field.

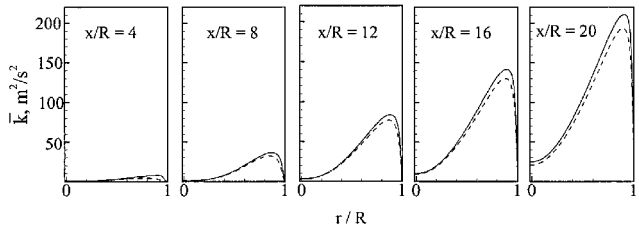

Fig. 6 Radial distributions of turbulent kinetic energy at various axial locations for f = 943 Hz and ε = 0.02: - - - -, without forced oscillation, and ——, with forced oscillation.

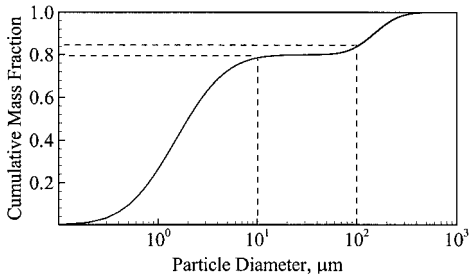

Fig. 7 Bimodal log-normal distribution of particle size.

VI. Two-Phase Flow Interactions with Acoustic Oscillations

Particle Size Distribution in Rocket Motor

Based on Salita's study of several operational metallized solid propellants,[42] the size distribution of aluminum particles in a rocket motor typically follows a bimodal log-normal profile. The cumulative mass distribution can be expressed with the following formula:

$$f(d_p) = \tfrac{1}{2}\left\{\left[1 + \mathrm{erf}\left(z_1/\sqrt{2}\right)\right](1 - f_0) + \left[1 + \mathrm{erf}\left(z_2/\sqrt{2}\right)\right] f_0\right\} \quad (22)$$

where

$$z_1 = (1/\sigma_1)\log_{10}(d_p/d_{m1}), \qquad z_2 = (1/\sigma_2)\log_{10}(d_p/d_{m2}) \quad (23)$$

with d_{m1} and d_{m2} the mass-mean diameters, σ_1 and σ_2 the standard deviations for the two modes, respectively, and f_0 the modal mass fraction. For the first mode, which accounts for 80% of the total mass, the mass-mean diameter and standard deviation are found to be 1.5 μm and 0.2, respectively, regardless of pressure, quench distance, quench liquid, and propellant. For the second mode, the standard deviation is about 0.4 and is independent of the factors just listed, but the mass-mean diameter decreases with increasing pressure. In the present work we choose 150 μm, following the work of Sabnis et al.[11] The resultant cumulative mass distribution is shown in Fig. 7. Small particles comprising oxidized aluminum appear as smoke, wheras large particles are composites of burned and unburned aluminum.

Two different kinds of particle size distribution are treated in the present study. The first case assumes a uniform size distribution throughout the entire injection surface, so that the particle size effect can be carefully examined. Two characteristic diameters in Fig. 7 are considered: 1) 10 μm, the upper limit of the particle size in the first mode, accounting for 80% of the total mass, and 2) 100 μm, a typical particle size close to the lower limit in the second mode. In the second case, the particle size follows the bimodal log-normal distribution given in Fig. 7. The quantity of particles at the injection surface is determined jointly by the mass distribution function and mass flow rate of particles.

Particles are injected in groups of parcels from 70 locations, which are uniformly distributed along the side wall of the chamber. The mass flow rate of each parcel is determined by

$$\dot{m}_{pi} = n_i\left(\tfrac{4}{3}\pi d_{pi}^3 \rho_p\right) \cdot f_p \quad (24)$$

where n_i and d_{pi} are the number and diameter of particles in parcel i, respectively, and f_p is the particle injection frequency. An algorithm described in Ref. 43 is employed to ensure that the injected particles follow the prespecified size-distribution function. In principle, the particle injection velocity falls in the range between the propellant burning rate and the corresponding gas-phase velocity. Because the void fraction ϕ is assumed to be unity and the particles are treated as a discrete phase, the particle velocity at the injection surface does not influence the particle-phase mass flow. Under stationary conditions, Madabhushi et al.[44] studied the sensitivity of particle dynamics to the injection velocity by varying the latter between 1 and 25% of the gas velocity at the surface. The result shows that the particle dynamics is insensitive to the injection velocity. Vuillot et al.[14] examined the effect of the particle injection velocity on the gas-phase flowfield in an oscillatory environment, in which the particle injection velocity was varied from 0.4 to 83% of the gas velocity. The resultant changes in the attenuation and dispersion of the acoustic wave appear to be negligible. In light of its limited influence on the oscillatory flowfield, the particle velocity at the injection surface is fixed at 10% of the gas-phase velocity throughout the present study.

Acoustic- and Turbulent-Flow-Induced Particle Dispersion

Particle dispersion due to acoustic oscillation can be conveniently examined through snapshots of the particle field, from which a general description of the influence of acoustic motion on particle dynamics can be conceived. Figure 8 shows the result for the short chamber in which the flow is predominantly laminar. For a uniform distribution of particle diameter of 100 μm, the streak lines originating from the surface can be clearly defined in the bulk of the flowfield, except in the middle of the chamber where a large excursion of acoustic velocity takes place. The deviation from the mean path appears to be limited because of the large particle inertia. The lack of interweaving of trajectories suggests poor mixing among particles. The situation with small particles with a diameter of 10 μm, however, is drastically different. Although the streak lines can still be identified near the surface, they experience large excursions of oscillations in the core region, leading to a chaotic particle field. The phenomenon can be explained in terms of the acoustic

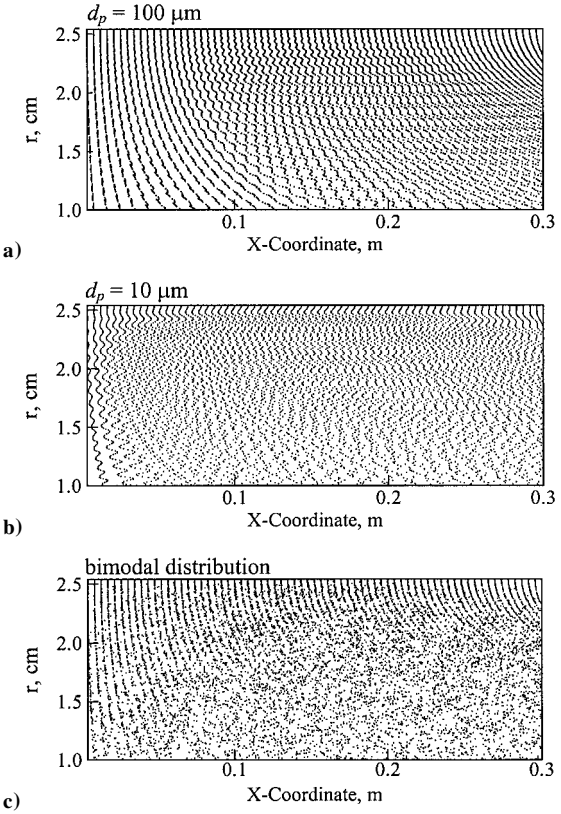

Fig. 8 Snapshots of particle field in laminar flow with first longitudinal mode of acoustic oscillation (f = 1885 Hz): a) d_p = 100 μm, b) d_p = 10 μm, and c) bimodal size distribution.

characteristic time τ_a, defined as the time period of the acoustic wave, and the particle momentum relaxation time τ_v. In the present case, τ_a is approximately 0.5 ms, and $\tau_v = 0.1$ and 10 ms for the small ($d_p = 10\ \mu$m) and large ($d_p = 100\ \mu$m) particles, respectively. Clearly, small particles have a much shorter relaxation time than the acoustic characteristic time and, consequently, can closely follow the local flow oscillation. Large particles are much less responsive and basically stay with their steady-state trajectories. The snapshot of the particle field for the case with a bimodal size distribution is given in Fig. 8c. The distinct streak lines observed in the earlier two cases become obscured. The particles are well mixed in the core region. Based on this observation, we may conclude that collisions among particles with a uniform size distribution are unlikely to take place in a laminar flowfield with acoustic excitation. A nonuniform distribution of particles is required for collisions to occur. The wider the range of particle size is, the greater the opportunity is for particles to collide. The situation, however, may become fundamentally different in turbulent flows in which turbulent dispersion may substantially modify the particle dynamics.

The extent of particle dispersion by turbulence can be characterized by the product of the mean squared fluctuating velocity and the integral timescale of the particle.[30] Both parameters are closely related to the inertia of a particle. The particle integral timescale measures the time interval over which the particle velocity is correlated with its initial velocity before being influenced by turbulence. Thus, larger particles with greater inertia have higher values of integral time. Figure 9 shows the snapshots of the particle fields with two different uniform size distributions, that is, 10 and 100 μm in diameter, in the long chamber under the first longitudinal mode of acoustic oscillation. Well-defined particle streak lines are clearly observed in the upstream laminar flow region for both cases. Small particles can follow acoustic wave motions because of their low momentum inertia. In the downstream turbulent flow region, however, the organized paths of small particles are destroyed and interweaved with their adjacent ones, resulting in a well-mixed homogeneous particle field. Turbulence dispersion exerts a strong influence and may even exceed the impact of acoustic wave on particle motion, depending on the local acoustic velocity field. For large particles, the streak lines remain in shapes similar to their laminar counterparts. The high inertia of the particles renders the turbulence dispersion effect comparatively small.

Effect of Particles on Acoustic Flowfield

The effect of particles on oscillatory flow motions can be conveniently demonstrated by considering the instantaneous fluctuating

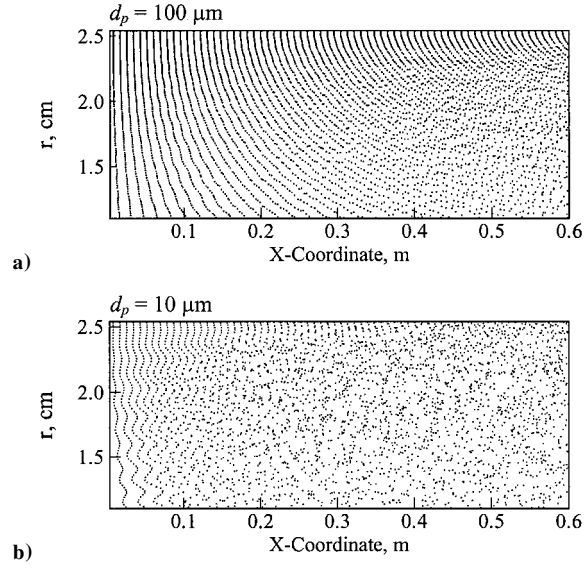

Fig. 9 Snapshots of particle field in turbulent flow with first longitudinal mode of acoustic oscillation (f = 943 Hz): a) d_p = 100 μm and b) d_p = 10 μm.

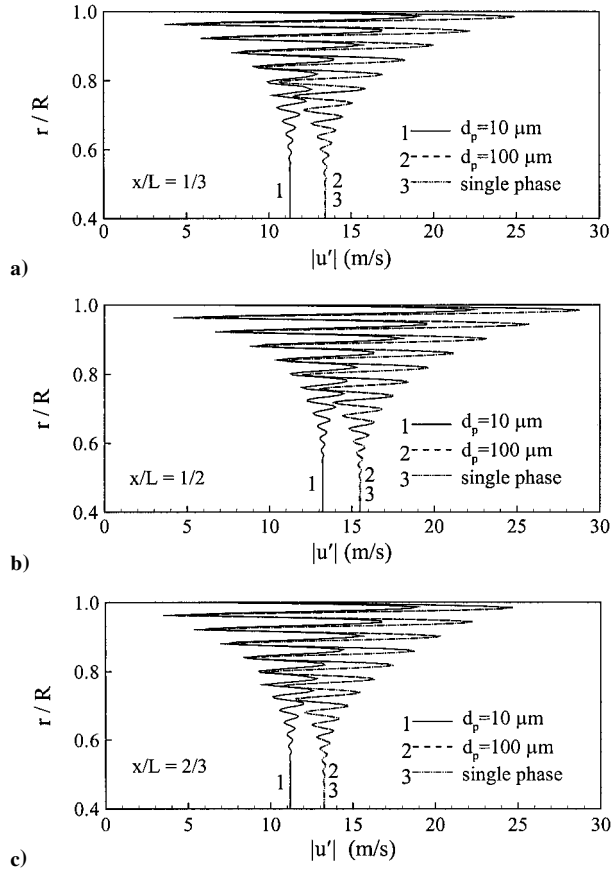

Fig. 10 Amplitudes of axial velocity fluctuation in laminar flow with first longitudinal mode of acoustic oscillation (f = 1885 Hz, C_m = 0.2, and ε = 0.02) at a) $x/L = \frac{1}{3}$, b) $x/L = \frac{1}{2}$, and c) $x/L = \frac{2}{3}$.

velocity field. Figures 10 and 11 present the radial distributions of the amplitude and phase of the axial velocity fluctuation, respectively, in the short chamber ($L = 0.3$ m), where the mean flow is basically laminar. The particle mass fraction C_m is 0.2, and the particle injection velocity is 0.1 m/s. The acoustic oscillation is of the first longitudinal mode with a frequency of 1885 Hz. Two distinct regions are noted. The first one encompasses the near-wall flowfield ($r/R > 0.6$), where both the acoustic and vorticity oscillations prevail. In the second region ($r/R \leq 0.6$), the vorticity wave diminishes due to viscous dissipation, and the oscillatory field is solely dominated by the acoustic motion. In general, particles tend to reduce the amplitude of acoustic waves through their momentum and thermal exchanges with surrounding gases, a phenomenon that has been discussed in connection with Fig. 2. The net effect on the acoustic-wave attenuation, dispersion, and impedance depends on the particle loading density, momentum and thermal relaxation times, and acoustic oscillation frequency. Small particles are more effective in modifying the acoustic impedance ($\overline{\rho a}$) characteristics because they can easily reach thermodynamic equilibrium with the local gaseous field and, consequently, increase the mixture compressibility. The situation with large particles, however, is drastically different. The disparity of particle relaxation and acoustic timescales may decouple the oscillatory processes in the two phases. As a result, particles exert negligible influence on the acoustic impedance of the two-phase flow. The acoustic velocity in a mixture with large particles is identical to its counterpart in a pure gas flowfield.

With the assumption of an ideal mixture, the acoustic velocity amplitude can be related to the acoustic pressure amplitude as follows:

$$|u'| = |p'|/\overline{\rho a} \tag{25}$$

where the effective mixture density $\bar{\rho}$ and speed of sound $\bar{a}$ are determined using Eqs. (19) and (18), respectively. For small particles with $d_p = 10\ \mu$m, the momentum relaxation time of 0.1 ms is

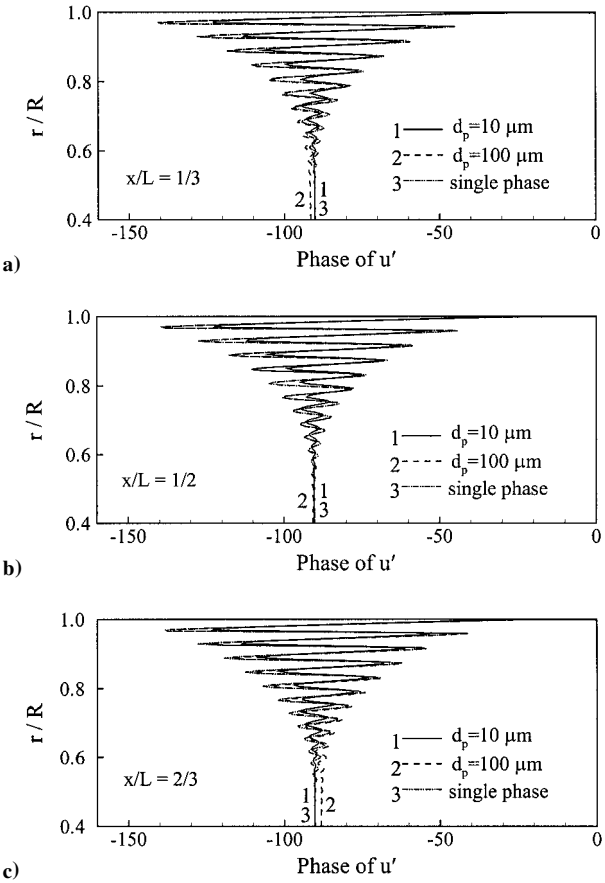

Fig. 11 Phases of axial velocity fluctuation in laminar flow with first longitudinal mode of acoustic oscillation (f = 1885 Hz, C_m = 0.2, and ε = 0.02) at a) $x/L = \frac{1}{3}$, b) $x/L = \frac{1}{2}$, and c) $x/L = \frac{2}{3}$.

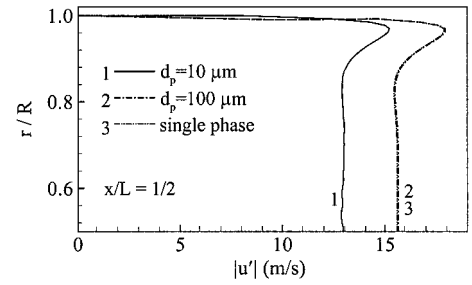

Fig. 12 Amplitude of axial velocity fluctuation in turbulent flow with first longitudinal mode of acoustic oscillation (f = 3770 Hz, C_m = 0.2, and ε = 0.02) at $x/L = \frac{1}{2}$.

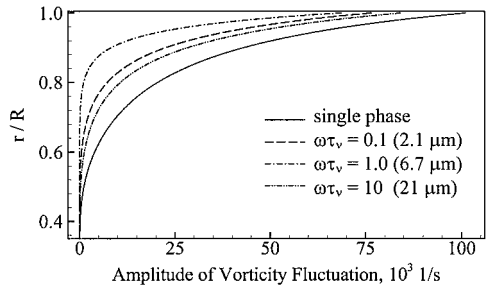

Fig. 13 Analytical solution of amplitude of vorticity fluctuation in laminar flow with first longitudinal mode of acoustic oscillation (f = 1885 Hz, C_m = 0.2, and ε = 0.02) at $x/L = \frac{1}{2}$.

much less than the acoustic time of 0.5 ms. The effective mixture density $\bar{\rho}$ approaches its asymptotic value of $\bar{\rho} = \rho(1 + C_m)$ for infinitesimally small particles or low frequencies. For large particles with $d_p = 100$ μm, $\bar{\rho}$ and $\bar{a}$ remain the same as those of a single gas flow. The numerical results shown in Fig. 10 are in excellent agreement with the analytical solution given by Eq. (25). The small deviation of less than 0.1% may arise from numerical errors due to grid resolution. The maximum velocity amplitude occurs at the middle of the chamber, with $|u'|_{\max} = 13.2$ m/s for $d_p = 10$ μm and 15.4 m/s for $d_p = 100$ μm. The phase distributions given in Fig. 11 indicate that the acoustic pressure leads the acoustic velocity by a phase angle of 90 deg for such a standing longitudinal wave system. The small deviation associated with large particles, $d_p = 100$ μm, may be caused by the dispersion effect and numerical error. The rapid phase variation in the near-wall region arises from the vorticity wave, as detailed in Refs. 5, 6, and 8. An analytical study by Thomas et al.[45] indicates that the damping effect of particles on acoustic motion is reduced by the presence of the vortical wave. The extent of this reduction can be characterized jointly by the particle size and the acoustic Strouhal number defined as $Sr \equiv Rk_n/M_b$, with R, k_n, and M_b being the chamber radius, wave number, and injection Mach number, respectively. Because the Strouhal number is on the order of 100 in the present work, the effect of vorticity on particle acoustic damping is minimal, about 1% for $d_p = 10$ μm and 20% for $d_p = 100$ μm. Because the acoustic damping effect of large particles is already small, the net reduction associated with the vortical wave is barely observed, as also suggested in Ref. 45.

The preceding analysis of acoustic impedance and velocity field remains valid even for a turbulent flow. Figure 12 shows the radial profiles of the amplitude of the axial velocity fluctuation at the midsection of the full-length chamber ($L = 0.6$ m), where the flow is turbulent in the downstream region. All of the injection conditions and particle mass fraction are identical to those for the short chamber. As in the laminar flow case, the influence of large particles on the acoustic velocity is negligible because of their high inertia, and small particles can effectively reduce the velocity oscillation. The calculated velocity fluctuation amplitude at the acoustic pressure nodal point ($x/L = 0.5$) is the same for both the short and full-length chambers. Turbulence exerts little influence on the acoustic wave structure. Its primary contribution lies in the dissipation of the vortical motion through the turbulence-enhanced eddy viscosity.

Effect of Particles on Vortical Flowfield

A theoretical basis is established to explore the interactions between particles and the vortical flow motions. Following the approach of Flandro,[5] the oscillatory velocity and temperature fields are split as follows:

$$\boldsymbol{u}' = \boldsymbol{u}_a + \boldsymbol{u}_v, \qquad T' = T_a + T_v \tag{26}$$

where the primed quantities represent fluctuating properties to first-order approximation and the subscripts a and v the acoustic and vortical modes, respectively. The equation governing the unsteady vortical motion in a two-phase mixture is derived by substituting Eq. (27) into the linearized momentum equation,

$$\frac{\partial \boldsymbol{u}_v}{\partial t} = -(\nabla \boldsymbol{u}_v \cdot \boldsymbol{U} - \boldsymbol{u}_v \times \nabla \times \boldsymbol{U} - \boldsymbol{U} \times \nabla \times \boldsymbol{u}_v) - \nu[\nabla \times \nabla \times \boldsymbol{u}_v] - \frac{\rho_s}{\rho}\frac{\mathrm{d}\boldsymbol{u}_{pv}}{\mathrm{d}t} \tag{27}$$

where $\boldsymbol{u}_{pv}$ is the particle fluctuating velocity arising from the vortical flow motion. Application of the Stokes flow approximation leads to the following equation of particle motion:

$$\frac{\mathrm{d}\boldsymbol{u}_{pv}}{\mathrm{d}t} = -\frac{18\mu}{\rho_s d_p^2}(\boldsymbol{u}_{pv} - \boldsymbol{u}_v) \tag{28}$$

Equations (27) and (28) provide an analytical framework for determining the oscillatory vortical field in a two-phase mixture. Figure 13 shows the result of the first longitudinal-mode oscillation in the short chamber ($L = 0.3$ m) at $x/L = \frac{1}{2}$. Three different

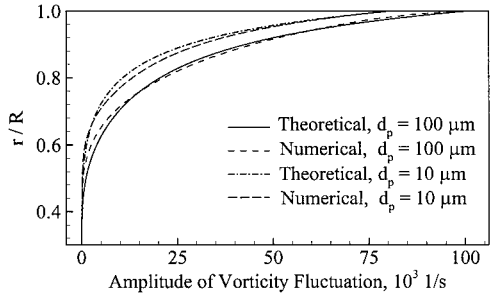

Fig. 14 Comparison between analytical and numerical solutions of amplitude of vorticity fluctuation in laminar flow with first longitudinal mode of acoustic oscillation (f = 1885 Hz, C_m = 0.2, and ε = 0.02) at $x/L = \frac{1}{2}$.

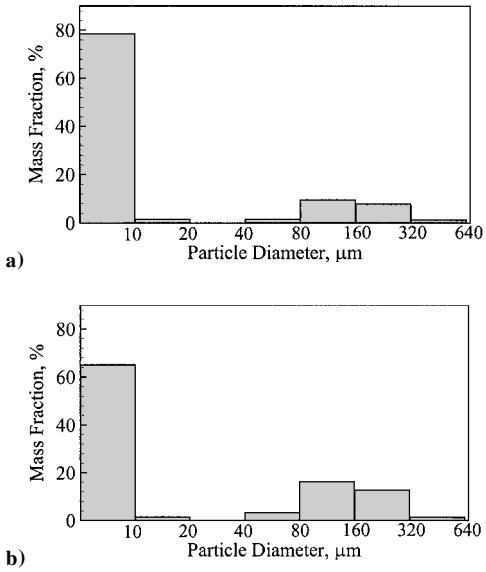

Fig. 15 Particle size distribution in laminar flow with first longitudinal mode of acoustic oscillation (f = 1885 Hz, C_m = 0.2, and ε = 0.02) at a) injection surface and b) chamber exit.

particle sizes are considered, with $\omega\tau_v = 0.1$, 1.0, and 10. The particle mass fraction C_m remains fixed at 0.2. The damping effect of particles on the vortical flow motion is clearly observed. In particular, an optimum size with $d_p = 6.7$ μm, corresponding to $\omega\tau_v = 1.0$, is obtained to exert the maximum dissipation on flow oscillations. Figure 14 shows good agreement between the analytical and numerical predictions.

Particle Intraphase Interaction

Particle intraphase interactions under the influence of acoustic oscillations are studied by comparing the particle size distributions at the injection surface and the chamber exit. Figure 15 shows the result for the short chamber with the first longitudinal mode of acoustic oscillation. The particles follow a bimodal size distribution at the injection surface as described earlier. The distribution at the chamber exit is spatially averaged in the radial direction. The particle mass fraction C_m is 0.2. As a consequence of particle collision and coalescence due to flow oscillations, a considerable decrease in mass fraction for particles less than 10 μm is observed at the chamber exit, whereas the mass-mean diameter increases from 35 to 60 μm. In contrast, for particles with an initially uniform size distribution, the change of mass-mean diameter appears limited, which indicates negligible intraphase interactions among particles.

Turbulence may substantially modify the particle dynamics through its dispersion effect. Even for particles with a uniform size distribution, collision, coalescence, and agglomeration may occur in regions with strong turbulence intensity, as evidenced in Fig. 9.

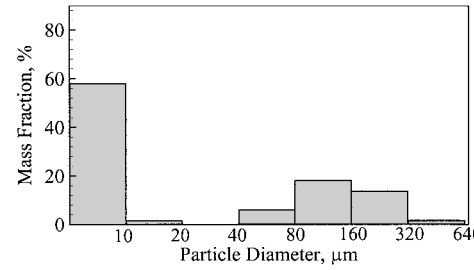

Fig. 16 Particle size distribution in turbulent flow with first longitudinal mode of acoustic oscillation (f = 943 Hz, C_m = 0.2, and ε = 0.02) at chamber exit.

To investigate the particle intraphase interactions in a turbulent flow, we consider the injection of particles with a bimodal distribution to the full chamber ($L = 0.6$ m). Figure 16 shows the particle size distribution at the chamber exit. The mass fraction of small particles with $d_p \leq 10$ μm decreases from 65% in a laminar flow to 58% in the present turbulent flow case, and the mass-mean diameter increases from 60 to 71 μm. Turbulence dispersion and the increased particle residence time in the long chamber indeed enhance the probability of particle collision and ensued agglomeration. Note that, in both the laminar and turbulent cases, the particle size at the chamber exit remains a bimodal distribution, but with a different mean value for each mode. Coalescence mainly occurs between small particles of the first mode and large particles of the second mode. The mass fractions of medium-size particles, that is, $10 \leq d_p \leq 20$ μm, and large-size particles, that is, $320 \leq d_p \leq 640$ μm, are not changed, suggesting that agglomeration among particles within each mode is insignificant. To further clarify this issue, particles with a uniform size distribution of $d_p = 10$ μm are injected. The mass-mean diameter at the chamber exit only increases slightly to 10.1 μm. Coalescence among particles with the same size is just not effective in spite of the turbulence dispersion effect. This finding is consistent with the observation by Salita[33] that the collision of micrometer-size Al_2O_3 with large agglomerates results in nearly 100% coalescence, whereas the large-particle collision efficiency is only about 5%.

Summary

A comprehensive numerical analysis based on a combined Eulerian–Lagrangian approach has been established to study the two-phase flow interactions in solid-propellant rocket motors with acoustic oscillations. The model treats the complete gas-phase conservation equations in axisymmetric coordinates and the particle equations of motion and energy conservation. The interphase interactions between the gas and particle phases are modeled by means of mass, momentum, and energy exchanges. Turbulence closure for the gas phase is achieved using a modified two-layer model. Also included in the formulation is the turbulence dispersion effect on particle dynamics.

As part of the model validation effort, the analysis was first applied to investigate the acoustic wave attenuation and dispersion in a two-phase mixture of gas and particles. The results show good agreement with the linear theory of Epstein and Carhart,[36] in terms of attenuation coefficient, acoustic velocity, and acoustic impedance as a function of frequency, particle relaxation times and mass fraction, and gas-phase properties. The numerical analysis was then implemented to examine the two-phase flow interactions with externally imposed acoustic wave motions in an operational rocket motor previously studied by Culick and Yang.[3] Strong coupling among acoustic oscillations, vortical motions, turbulent fluctuations, and particle dynamics is observed. Acoustic waves tend to enhance turbulence intensity and give rise to an early transition from laminar to turbulent flow through energy transfer from the organized oscillatory field to the broadband turbulent flowfield. On the other hand, turbulence can effectively increase the eddy viscosity and, consequently, dissipate the vortical wave originating from the injection surface.

The effect of particles on the oscillatory flowfield is mainly dictated by their relaxation times, defined as the time required for a particle to reach equilibrium with the surrounding gas in response to a local flow variation, and the acoustic wave characteristic time. A maximum dissipation of flow oscillations occurs when these timescales become comparable. Small particles exert little influence on acoustic wave attenuation, but substantially modify the acoustic wave speed and impedance through its effect on mixture compressibility. Large particles with characteristic times disparate from acoustic times tend to decouple from the local flow oscillations and, consequently, render a negligible effect on wave motions.

Turbulent dispersion is mainly observed on small particles. In the present study, the intraphase interactions among particles such as collision and coalescence occur primarily for particles with different sizes. Agglomeration within each particle-size group appears to be insignificant, a phenomenon confirmed by Salita in his experiments on particle collisions in simulated motor environments.

Acknowledgments

This work was sponsored in part by Pennsylvania State University, and in part by California Institute of Technology Multidisciplinary University Research Initiative program under the Office of Naval Research Grant N00014-95-1-1338.

References

[1]Price, E. W., "Solid Rocket Combustion Instability—An American Historical Account," *Unsteady Burning and Combustion Stability of Solid-Propellants*, edited by L. De Luca, E. W. Price, and M. Summerfield, Vol. 143, Progress in Astronautics and Aeronautics, AIAA, Washington, DC, 1992, pp. 1–16.

[2]Ramohalli, K., "Technologies and Techniques for Instability Suppression in Motors," *Unsteady Burning and Combustion Stability of Solid-Propellants*, edited by L. De Luca, E. W. Price, and M. Summerfield, Vol. 143, Progress in Astronautics and Aeronautics, AIAA, Washington, DC, 1992, pp. 805–848.

[3]Culick, F. E. C., and Yang, V., "Prediction of the Stability of Unsteady Motions in Solid-Propellant Rocket Motors," *Unsteady Burning and Combustion Stability of Solid-Propellants*, edited by L. De Luca, E. W. Price, and M. Summerfield, Vol. 143, Progress in Astronautics and Aeronautics, AIAA, Washington, DC, 1992, pp. 719–779.

[4]Nickerson, G. R., Culick, F. E. C., and Dang, L. G., "Standard Stability Prediction Method for Solid Rocket Motors, Axial Mode Computer Program, User's Manual," Software and Engineering Associates, Inc., AFRPL TR-83-017, Air Force Rocket Propulsion Lab., Edwards Air Force Base, CA, 1983.

[5]Flandro, G. A., "Effects of Vorticity on Rocket Combustion Instability," *Journal of Propulsion and Power*, Vol. 11, No. 4, 1995, pp. 607–625.

[6]Flandro, G. A., Cai, W., and Yang, V., "Turbulent Transport in Rocket Motor Unsteady Flowfield," *Solid Propellant Chemistry, Combustion and Motor Interior Ballistics*, Vol. 185, edited by V. Yang, T. B. Brill, and W. Z. Ren, Progress in Astronautics and Aeronautics, AIAA, Reston, VA, 2000, pp. 837–858.

[7]Apte, S., and Yang, V., "Unsteady Flow Evolution in Porous Chamber with Surface Mass Injection, Part 1: Free Oscillation," *AIAA Journal*, Vol. 39, No. 8, 2001, pp. 1577–1586.

[8]Apte, S., and Yang, V., "Unsteady Flow Evolution in Porous Chamber with Surface Mass Injection, Part 2: Acoustic Excitation," *AIAA Journal*, Vol. 40, No. 2, 2002, pp. 244–253.

[9]Salita, M., "Deficiencies and Requirements in Modeling of Slag Generation in Solid Rocket Motors," *Journal of Propulsion and Power*, Vol. 11, No. 1, 1995, pp. 10–23.

[10]Johnston, W. A., Murdock, J. W., Koshigoe, S., and Than, P. T., "Slag Accumulation in the Titan SRMU," *Journal of Propulsion and Power*, Vol. 11, No. 5, 1995, pp. 1012–1020.

[11]Sabnis, J. S., "Numerical Simulation of Distributed Combustion in Solid Rocket Motors with Metallized Propellants," *Journal of Propulsion and Power*, Vol. 19, No. 1, 2003.

[12]Cesco, N., "Etude et modélisation de l'écoulement diphasique à l'interieur des propulseurs à poudre," Ph.D. Dissertation, Ecole Nationale Supérieure de l'Aéroautique et de l'Espace, Toulouse, France, Nov. 1997.

[13]Dupays, J., Prevost, M., Tarrin, P., and Vuillot, F., "Effects of Particulate Phase on Vortex Shedding Driven Oscillations in Solid Rocket Motors," AIAA Paper 1996-3248, July 1996.

[14]Vuillot, F., Basset, T., Dupays, J., Daniel, E., and Lupoglazoff, N., "2D Navier–Stokes Stability Computations for Solid Rocket Motors: Rotational, Combustion, and Two-Phase Flow Effects," AIAA Paper 1997-3326, July 1997.

[15]Daniel, E., and Thévand, N., "Stability of Acoustic Wave in Two-Phase Dilute Flow with Mass Transfer," *AIAA Journal*, Vol. 39, No. 11, 2001, pp. 2121–2130.

[16]Dupays, J., Fabignon, Y., Villedieu, P., Lavergne, G., and Estivalezes, J. L., "Some Aspects of Two-Phase Flows in Solid-Propellant Rocket Motors," *Solid Propellant Chemistry, Combustion and Motor Interior Ballistics*, edited by V. Yang, T. B. Brill, and W. Z. Ren, Vol. 185, Progress in Astronautics and Aeronautics, AIAA, Reston, VA, 2000, pp. 859–883.

[17]Apte, S., and Yang, V., "Turbulent Flame Dynamics of Homogeneous Solid Propellant in a Rocket Motor," *Proceedings of the Combustion Institute*, Vol. 28, 2000, pp. 903–910.

[18]Apte, S., and Yang, V., "Unsteady Flow Evolution and Combustion Dynamics of Homogeneous Solid Propellant in a Rocket Motor," *Combustion and Flame*, Vol. 131, 2002, pp. 110-131.

[19]Tseng, I.-S., and Yang, V., "Combustion of a Double-Base Homogeneous Propellant in a Rocket Motor," *Combustion and Flame*, Vol. 96, No. 4, 1994, pp. 325–342.

[20]Cousteix, J., Desopper, A., and Houdeville, R., "Structure and Development of a Turbulent Boundary Layer in an Oscillating External Flow," *Proceedings of First International Symposium on Turbulent Shear Flows*, Springer-Verlag, Berlin, 1979, pp. 154–171.

[21]Ramaprian, B. R., and Tu, S. W., "An Experimental Study of Oscillatory Pipe Flow at Transitional Reynolds Numbers," *Journal of Fluid Mechanics*, Vol. 100, No. 3, 1980, pp. 513–544.

[22]Fan, S., and Lakshminarayana, B., "Low-Reynolds-Number k–ε Model for Unsteady Turbulent Boundary-Layer Flows," *AIAA Journal*, Vol. 31, No. 10, 1993, pp. 1777-1784.

[23]Kovalnogov, N., "Unsteady Heat Transfer and Friction in Internal Axisymmetric Flows with Longitudinal Pressure Gradients," *Heat Transfer Research*, Vol. 25, No. 3, 1993, pp. 304–307.

[24]Cai, W., "Two-Phase Flow Interactions and Combustion of AP/HTPB Composite Propellants in Rocket Motors with Acoustic Oscillations," Ph.D. Dissertation, Dept. of Mechanical Engineering, Pennsylvania State Univ., University Park, PA, 2001.

[25]Mostafa, A. A., and Mongia, H. C., "On the Interaction of Particles and Turbulent Fluid Flow," *International Journal of Heat and Mass Transfer*, Vol. 31, No. 10, 1988, pp. 2063–2075.

[26]Faeth, G. M., "Evaporation and Combustion of Sprays," *Progress in Energy and Combustion Science*, Vol. 9, 1983, pp. 1–76.

[27]Mei, R., "An Approximate Expression for the Shear Lift on a Spherical Particle at Finite Reynolds Number," *International Journal of Multiphase Flow*, Vol. 18, No. 1, 1992, pp. 145–147.

[28]Putnam, A., "Integratable Form of Droplet Drag Coefficient," *American Rocket Society Journal*, Vol. 31, 1961, pp. 1467–1468.

[29]Whitaker, S., "Forced Convective Heat-Transfer Correlations for Flows in Pipes, Past Flat Plates, Single Cylinders, Single Spheres, and Flows in Packed Beds and Tube Bundles," *AIChE Journal*, Vol. 18, 1972, p. 361.

[30]Shuen, J. S., Chen, L. D., and Faeth, G. M., "Evaluation of a Stochastic Model of Particle Dispersion in a Turbulent Round Jet," *AIChE Journal*, Vol. 29, 1983, pp. 167–170.

[31]Chen, X.-Q., and Pereira, J. C. F., "Prediction of Evaporating Spray in Anisotropically Turbulent Gas Flow," *Numerical Heat Transfer*, Pt. A, No. 27, 1995, pp. 143–162.

[32]Burry, G., and Bergeles, G., "Dispersion of Particles in Anisotropic Turbulent Flows," *International Journal of Multiphase Flow*, Vol. 19, No. 4, 1993, pp. 651–664.

[33]Salita, M., "Use of Water and Mercury Droplets to Simulate Al_2O_3 Collision/Coalescence in Rocket Motor," *Journal of Propulsion and Power*, Vol. 7, 1991, pp. 505–512.

[34]Lefebvre, A. H., *Atomization and Sprays*, Hemisphere, New York, 1989.

[35]Hsieh, S. Y., and Yang, V., "A Preconditioned Flux-Differencing Scheme for Chemically Reacting Flows at All Mach Numbers," *International Journal of Computational Fluid Dynamics*, Vol. 8, 1997, pp. 31–49.

[36]Epstein, P. S., and Carhart, R. R., "The Absorption of Sound in Suspensions and Emulsions, I. Water Fog in Air," *Journal of Acoustic Society of America*, Vol. 25, No. 3, 1953, pp. 553–565.

[37]Zink, J. W., and Delsasso, L. P., "Attenuation and Dispersion of Sound by Solid Particles Suspended in a Gas," *Journal of Acoustic Society of America*, Vol. 30, No. 6, 1958, pp. 765–771.

[38]Temkin, S., "Attenuation and Dispersion of Sound in Dilute Suspensions of Spherical Particles," *Journal of Acoustical Society of America*, Vol. 108, No. 1, 2000, pp. 126–146.

[39]Temkin, S., Erratum "Attenuation and Dispersion of Sound in Dilute Suspensions of Spherical Particles," *Journal of Acoustical Society of America*, Vol. 111, No. 2, 2002, pp. 1126–1128.

[40]Beddini, R. A., "Injection Induced Flows in Porous-Walled Ducts," *AIAA Journal*, Vol. 24, No. 11, 1986, pp. 1766–1773.

[41]Dunlap, R., Blackner, A. M., Waugh, R. C., Brown, R. S., and Willoughby, P. G., "International Flowfield Studies in a Simulated Cylindrical Port Rocket Chamber," *Journal of Propulsion and Power*, Vol. 8, No. 6, 1992, pp. 1167–1176.

[42]Salita, M., "Quench Bomb Investigation of Al_2O_3 Formation from Solid Rocket Propellants (Part II): Analysis of Data," *Proceedings of 25th JANNAF Combustion Meeting*, CPIA Publ., Chemical Propulsion Information Agency, Johns Hopkins University, Laurel, MD, Oct. 1988.

[43]Press, W. H., Teukosky, S. A., Vetterling, W. T., and Flannery, B. P., *Numerical Recipes*, Vol. 1, 2nd ed., Cambridge Univ. Press, Cambridge, England, U.K., pp. 281–286.

[44]Madabhushi, R. K., Sabnis, J. S., de Jong, F. J., and Gibeling, H. J., "Calculation of Two-Phase Aft-Dome Flowfield in Solid Rocket Motors," *Journal of Propulsion and Power*, Vol. 7, No. 2, 1991, pp. 178–184.

[45]Thomas, H. D., Flandro, G. A., and Flanagan, S. N., "Effects of Vorticity on Particle Damping," AIAA Paper 1995-2736, July 1995.